



Nanofluid flow and MHD mixed convection inside a vertical annulus with moving walls and transpiration considering the effect of Brownian motion and shape factor

Ali Shakiba¹ · Asghar B. Rahimi²

Received: 31 January 2019 / Accepted: 15 March 2019 / Published online: 25 March 2019
© Akadémiai Kiadó, Budapest, Hungary 2019

Abstract

In the present study, the exact solution of a nanofluid flow and mixed convection within a vertical cylindrical annulus with suction/injection, which is adjacent to the radial magnetic field, is presented with regard to the motion of cylinders' walls. The impact of Brownian motion and shape factor on the thermal state of CuO–water nanofluid is also considered. The influence of such parameters as Hartmann number, mixed convection parameter, suction/injection, volume fraction of nanoparticles and motion of cylinders' walls on flow and heat transfer is probed. The results show that the shape of the nanoparticles could change the thermal behavior of the nanofluid and when the nanoparticles are used in the shape of a platelet, the highest Nusselt number is obtained (about 2.5% increase of Nusselt number on internal cylinders' wall comparison to spherical shape). The results shed light on the fact that if, for example, the external cylinder is stationary and the internal cylinder moves in the direction of z axis, the maximum and minimum heat transfer take place on the walls of internal and external cylinders, respectively (for $\eta = 300$, about 15% increase of Nusselt number on internal cylinders' wall). Furthermore, the enhancement of radius ratio between two cylinders increases the rate of heat transfer and decreases the shear stress on the internal cylinder's wall.

Keywords Vertical cylindrical annulus · Moving walls · Nanofluid · Magnetohydrodynamics (MHD) · Brownian motion · Mixed convective flow · Exact solution

List of symbols

A	Coefficient of velocity for inner cylinder
a	Radius of the inner cylinder (m)
B	Coefficient of velocity for outer cylinder
b	Radius of the outer cylinder (m)
B_0	Constant magnetic field (T), $B = (B_0 a)/r$
C_p	Specific heat ($\text{J kg}^{-1} \text{K}^{-1}$)
d_p	Nanoparticle diameter (m)
D_h	Hydraulic diameter, $D_h = 2(b - a)$
g	Gravitational acceleration (m s^{-2})
Ha	Hartman number
k	Thermal conductivity ($\text{W m}^{-1} \text{K}^{-1}$)
k_B	Boltzmann constant ($1.3806503 \times 10^{-23} \text{ J K}^{-1}$)

n	Shape factor
Nu	Nusselt number
p	Pressure (Pa)
P	Dimensionless pressure
Pr	Prandtl number
Q	Dimensionless volumetric flow rate
r	Axis in the cylindrical coordinates
Re	Reynolds number
S	Suction/injection parameter
T	Nanofluid temperature (K), $\Delta T = T_1 - T_0$
T_0	Wall temperature of outer cylinder (K)
T_1	Wall temperature of inner cylinder (K)
u	Velocity in z direction (m s^{-1})
u_0	Reference constant velocity (m s^{-1})
u_m	Mean velocity (m s^{-1})
V	Velocity in r direction (m s^{-1})
z	Axis in the cylindrical coordinates

✉ Asghar B. Rahimi
rahimiab@um.ac.ir.com

¹ Department of Mechanical Engineering, Ferdowsi University of Mashhad, Mashhad, Iran

² Faculty of Engineering, Ferdowsi University of Mashhad, P.O. Box No. 91775-1111, Mashhad, Iran

Greek letters

α_T	Thermal diffusivity ($\text{m}^2 \text{s}^{-1}$), $\alpha_T = k/(\rho \cdot C_p)$
β	Thermal expansion coefficient ($1/\text{K}$)

η	Mixed convection parameter
θ	Dimensionless temperature of nanofluid
λ	Ratio of the radius between two cylinders
μ	Dynamic viscosity (kg ms^{-1})
ρ	Density (kg m^{-3})
ν	Kinematic viscosity ($\text{m}^2 \text{s}^{-1}$), $\nu = \mu/\rho$
σ	Electrical conductivity ($\text{m}^{-1} \Omega^{-1}$)
τ	Dimensionless shear stress
ϕ	Particle volume fraction

Subscripts

l	Value on inner wall
b	Bulk temperature
eff	Effective characteristic
f	Pertaining to base fluid
m	Mean value
nf	Nanofluid
p	Nanoparticles
λ	Value on outer wall

Introduction

Mixed convection investigation in an annulus with suction/injection has attracted many researchers' attention due to diverse applications. Cooling systems of electrical appliances, heat exchangers, food processes, cooling of rotary machines and nuclear reactors are examples of industrial applications of this type [1]. In these applications, suction/injection was used to modify the heat transfer, and its effect on fluids' flow was investigated in format of different geometries, boundary conditions, as well as different solution methods. Avci and Aydın [2] carried out an investigation on flow and heat transfer of a vertical concentric microannulus. The authors revealed that increasing the mixed convection parameter intensifies heat transfer as rarefaction effects considered by the velocity slip and temperature jump in the slip flow regime decreased. Rahimi and Abedini [3] studied mixed convection of air in eccentric horizontal annuli. Their results demonstrated that flow and heat transfer are forcefully affected by the Raleigh number and eccentricity of the inner cylinder, and that three-dimensionality consideration was unavoidable. Jha et al. [4] investigated the effect of suction/injection on vertical annular microchannel. The authors found that skin friction declined on the inner porous cylinder's wall with growth of fluid-wall interaction parameter in case of injection at inner porous cylinder's wall and concurrent suction at outer porous cylinder's wall, while the result was just opposite at outer porous cylinder's wall. Shakiba and Rahimi [5] investigated the mixed convective flow of a fluid inside a vertical annulus with moving walls along

with transpiration and obtained exact solution showing improvement of heat transfer depending on different walls moving arrangements.

Some methods of heat transfer enhancement include changing the geometry, using nanoparticles and locating the fluid in a magnetic field. Low thermal conductivity of base fluids such as ethylene glycol, oils and water is one of the main causes that justifies the inefficiency of devices which use these fluids [6]. With the advancement of technology and the possibility of nanoscale particles, Choi et al. [6] were the first to suggest adding nanoparticles to the base fluid which were called "nanofluid." On the other hand, over the past two decades, investigation of electrically conductive fluids' magnetic properties has attracted the attention of many scientists. In many thermal industries, MHD has many important applications, such as chemical catalytic reactors, high-performance boilers, polymer and metallurgy, solar collectors and heat exchangers. The application of a desirable magnetic field in a nanofluid flow can greatly increase the rate of heat transfer [7]. Shakiba and Vahedi [8] numerically investigated the hydro-thermal properties of ferrofluid in a horizontal counter-current double pipe heat exchanger. The results demonstrated that when ferrofluid is exposed to a non-uniform transverse magnetic field, the Kelvin force is produced perpendicular to the nanofluid flow. Therefore, axial velocity profile is changed and a pair of vortices is created which lead to gain pressure drop, friction factor and heat transfer rate. Jha et al. [9] studied role of suction/injection on MHD natural convection flow in a vertical microchannel and the authors found that as suction/injection, fluid-wall interaction and rarefaction increased, the volume flow rate increased, while it decreased with increase in magnetic field intensity. Freidoonimehr and Rahimi [10] carried out entropy generation analysis induced by a stretching/shrinking sheet with transpiration. The authors found an exact solution for steady laminar MHD nanofluid flow and heat transfer. Results showed that the copper and the aluminum oxide nanoparticles have the largest and the lowest averaged entropy generation number, respectively, among all the nanoparticles considered. Singh et al. [1] obtained an exact solution for flow and heat transfer of a vertical concentric annulus, considering radial magnetic field. The authors concluded that both mass flow rate and skin friction decline due to increase in magnetic intensity. Mozayyeni and Rahimi [11] presented mixed convection flow of a fluid between two horizontally concentric cylinders. The authors showed that by considering radial magnetic field the flow oscillations in the annulus can be suppressed effectively. Moreover, it was found that due to existent of viscous dissipation, heat transfer increased and decreased on the external and internal cylinder, respectively. Mozayyeni and Rahimi [12]

investigated MHD fully developed mixed convection in an annulus with rotating outer cylinder. The authors realized that magnetic field suppressed the streamlines patterns, as well as temperature contours and the heat transfer. Other researches are available in existing studies [13, 14].

Brownian motion is a random and continuous motion of some suspended microscopic particles in a liquid or gas. By creating a nanofluid mixture, this accidental movement occurs due to the continuous collision of particles with fluid molecules and the exchange of momentum between them. This movement is known as the Brownian motion of particles. Malvandi and Ganji [15], in a numerical study, investigated the laminar flow and mixed convection heat transfer of alumina–water nanofluid in a vertical annulus. The authors considered Brownian motion and investigated the effects of nanoparticles migration on heat transfer and pressure drop. They also increased the efficiency of the system by using nanofluid and finding the optimal values for the radial ratio and the heat flux ratio. Dogonchi and Ganji [16] investigated Buoyancy nanofluid flow and heat transfer over a stretching sheet considering effect of Brownian motion, thermal radiation and magnetic field. Their results revealed that the fluid velocity and temperature distribution declined with the increase in radiation parameter. In addition, the authors revealed that skin-friction coefficient rose with the increase in magnetic parameter and it decreased with the increase in volume fraction of nanofluid. Furthermore, the Nusselt number decreased with the increase in magnetic parameter.

In many natural science problems, obtaining the exact solutions of mathematical equations can help researchers to understand qualitative features of many phenomena properly.

Despite numerous studies which were carried out concerning flow and heat transfer in the space between two cylinders with different solution methods, a limited number of them were probed into the suction/injection effects with the application of radial magnetic field and movement of cylinders.

The present work has intended to scrutinize various states affecting mixed convective flow within the vertical cylindrical annulus with complete range of moving walls for the selected nanofluid and as an exact solution which is for the first time. To do so, the Brownian motion of the CuO–water nanofluid has been taken into remarkable account. The effect of other parameters including ratio of the radius, suction/injection parameter, mixed convection parameter and Hartman number is also considered. The results show that by changing the effective parameters used in above, the flow and heat transfer of nanofluid can be controlled.

Problem statement

Mixed convection within a vertical annulus has been investigated in this study. In addition, the effects of moving walls, radial magnetic field and suction/injection on the flow and heat transfer of CuO–water nanofluid have been inspected. Since annulus length is infinite, all the parameters, except for the pressure gradient that is a function of z , are a function of r . As shown in Fig. 1, the internal and external cylinder radii are, respectively, a and b and the internal and external cylinder temperatures are, respectively, T_1 and T_0 , in which $T_1 > T_0$. The z axis is located along the annulus axis, and the r axis is perpendicular to it. The magnetic field is applied radially and with a size equal to $B_0 a/r$ to the annulus. It is assumed that the nanofluid's suction/injection is fulfilled through the walls of the annulus. The flow and heat transfer of the nanofluid have been investigated in different states, when the internal and external cylinders, or both move in different direction with constant velocities equal to Au_0 and Bu_0 , respectively.

Governing equations, boundary conditions and credibility

It is supposed that nanoparticles easily dispersed in fluid phase and thermal equilibrium state is established. Furthermore, nanoparticles are significantly small in sizes so

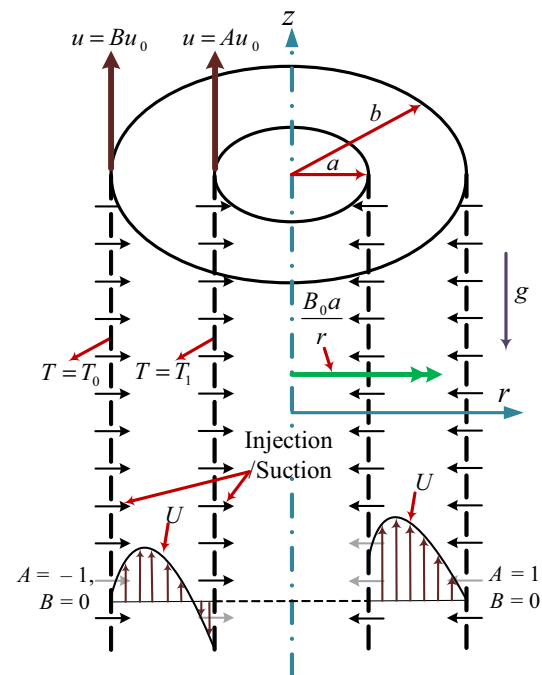


Fig. 1 Physical model and coordinate system of problem

slipping velocity between particles and continuous phase is assumed to be negligible.

Considering the laminar, steady, fully developed, Newtonian and incompressible nanofluid flow, using the Boussinesq approximation and applying no-slip condition on wall of cylinders, conservation equations, including continuity, momentum, energy, are expressed as Eqs. (1)–(3). Use of the thermophysical properties of nanofluid was required for writing these equations; on the other hand, the axial conduction of nanofluid and wall as well as the effects of compressibility and viscous dissipation has been ignored.

Continuity equation

$$\frac{1}{r} \frac{d}{dr} (rV) = 0, \quad (1)$$

Momentum equation

$$V \frac{du}{dr} = -\frac{1}{\rho_{nf}} \frac{dp}{dz} + \frac{\mu_{nf}}{\rho_{nf}} \frac{1}{r} \frac{d}{dr} \left(r \frac{du}{dr} \right) + g\beta_{nf}(T - T_0) - \frac{\sigma_{nf} B^2 u}{\rho_{nf}}, \quad (2)$$

Energy equation

$$\frac{k_{nf}}{(\rho C_p)_{nf}} \frac{1}{r} \frac{d}{dr} \left(r \frac{dT}{dr} \right) = V \frac{dT}{dr}. \quad (3)$$

In above equations, ρ_{nf} , β_{nf} , $(\rho C_p)_{nf}$ and σ_{nf} are density, thermal expansion coefficient, heat capacity and electrical conductivity of nanofluid accordingly and they are defined as:

$$\begin{aligned} \rho_{nf} &= \rho_f(1 - \phi) + \rho_s \phi \\ \beta_{nf} &= \beta_f(1 - \phi) + \beta_s \phi \\ (\rho C_p)_{nf} &= (\rho C_p)_f(1 - \phi) + (\rho C_p)_s \phi \\ \frac{\sigma_{nf}}{\sigma_f} &= 1 + \frac{3 \left(\frac{\sigma_s}{\sigma_f} - 1 \right) \phi}{\left(\frac{\sigma_s}{\sigma_f} + 2 \right) - \left(\frac{\sigma_s}{\sigma_f} - 1 \right) \phi} \end{aligned} \quad (4)$$

Various models have been proposed by various researchers for effective thermal conductivity and viscosity of nanofluids [17–20]. To calculate Brownian motion, the thermal conductivity of the nanofluid is considered to contain two parts. One assumes that all of the nanoparticles are stationary k_{static} , while other parts are the properties that arise from the Brownian motion of the particles $k_{Brownian}$. Hence, KKL (Koo–Kleinstreuer–Li) [21–23] has been used to calculate the effective thermal conductivity and viscosity of the nanofluid in addition to the effect of particle size, particle volume fraction, temperature dependence and base fluid properties are measured by considering the random motion of nanoparticles. The thermophysical properties of the nanofluid are given in Table 1.

The effective thermal conductivity and viscosity of the nanofluid on the basis of static and Brownian properties is defined in Eq. (5).

$$\begin{aligned} k_{eff} &= k_{static} + k_{Brownian} \\ \mu_{eff} &= \mu_{static} + \mu_{Brownian} = \mu_{static} + \frac{k_{Brownian}}{k_f} \times \frac{\mu_f}{Pr_f} \\ \frac{k_{static}}{k_f} &= \left[\frac{k_s + (n-1)k_f - (n-1)\phi_p(k_f - k_s)}{k_s + (n-1)k_f + \phi_p(k_f - k_s)} \right] \\ \mu_{static} &= \frac{\mu_f}{(1 - \phi)^{2.5}} \end{aligned} \quad (5)$$

$$k_{Brownian} = 5 \times 10^4 \phi \rho_f C_{p,f} \sqrt{\frac{k_b T}{\rho_p d_p}} g'(T, \phi, d_p)$$

In which Pr_f is Prandtl number of base fluid and is equal to 5.83. It should be noted that by taking into account the thermal interfacial resistance ($R_f = 4 \times 10^{-8} \text{ km}^2/\text{W}$) between nanoparticles and base fluid, according to Eq. (6) k_s will be replaced by $k_{s,eff}$ [26]. In Eq. (5), n is the shape factor, which is given in Table 2 for different shapes of nanoparticles.

$$R_f + \frac{d_p}{k_s} = \frac{d_p}{k_{s,eff}} \quad (6)$$

The experimental g' -function is also different for diverse nanofluids and base fluids. In this paper, for the base fluid water and CuO nanoparticles, this function is defined as Eq. (7) [21].

$$\begin{aligned} g'(T, \phi, d_p) &= (a_1 + a_2 \ln(d_p) + a_3 \ln(\phi) + a_4 \ln(\phi) \\ &\quad \ln(d_p) + a_5 \ln(d_p)^2) \ln(T) \\ &\quad + (a_6 + a_7 \ln(d_p) + a_8 \ln(\phi) \\ &\quad + a_9 \ln(\phi) \ln(d_p) + a_{10} \ln(d_p)^2) \end{aligned} \quad (7)$$

in which the coefficients a_i ($i = 0, 1, \dots, 10$) are selected according to the type of nanoparticles, and their values are given in Table 3.

The boundary conditions are as follows:

$$\begin{aligned} T = T_1 \quad u = Au_0 \quad r = a \\ T = T_0 \quad u = Bu_0 \quad r = b \end{aligned} \quad (8)$$

where A and B are constant coefficients. Given the above boundary conditions, if both of the constants are zero, they indicate a stagnant state for annulus.

Through solving Eq. (1), the velocity in the direction of r is achieved by Eq. (9):

$$V = \frac{-aV_0}{r} \quad (9)$$

Table 1 Thermophysical properties of water and CuO nanoparticles [24, 25]

	$\rho/\text{kg m}^{-3}$	$C_p/\text{J kg}^{-1} \text{K}^{-1}$	$k/\text{W mK}^{-1}$	$\beta \times 105/1 \text{K}^{-1}$	d_p/nm^{-1}	$\sigma/\Omega \text{m}^{-1}$
Water	997.1	4179	0.613	21	–	0.05
CuO	6500	540	18	29	45	5×10^7

Table 2 The values of shape factor for different shapes of nanoparticles

Shape	n
Spherical 	3
Platelet 	5.7
Cylinder 	4.8
Brick 	3.7

Energy equation

$$\frac{k_{nf} (\rho C_p)_{nf}}{k_f (\rho C_p)_f} \frac{1}{Pr} \frac{d}{dR} \left(R \frac{d}{dR} \theta(R) \right) + S \frac{d}{dR} \theta(R) = 0 \quad (12)$$

The aforementioned equations are solved using the following boundary conditions:

$$\begin{aligned} \theta = 1 \quad U = A \quad R = 1 \\ \theta = 0 \quad U = B \quad R = \lambda \end{aligned} \quad (13)$$

Mean velocity, which is taken into account as the reference velocity (u_0), is derived through Eq. (14) at any cross section of annulus. In addition, dimensionless volumetric flow rate (Q), which is deemed constant at any cross section of annulus, can be achieved through Eq. (15).

$$u_0 = u_m = \frac{\int_a^b u r dr}{\int_a^b r dr}, \quad (14)$$

$$Q = \int_1^\lambda R U(R) dR = \int_1^\lambda R dR = \frac{1}{2} (\lambda^2 - 1). \quad (15)$$

By employing the boundary conditions in Eq. (13) and solving Eqs. (11) and (12), the results of exact solution are obtained as Eqs. (16) and (17).

$$\theta(R) = \frac{-1 + \lambda^{\frac{Pr S_{2f}}{2n_f}} R^{-\frac{Pr S_{2f}}{2n_f}}}{-1 + \lambda^{\frac{Pr S_{2f}}{2n_f}}}, \quad (16)$$

$$U(R) = C_1 R^{\delta_1} + C_2 R^{\delta_2} + \delta_6 R^2 + \delta_7 R^{2 - \frac{Pr S_{2f}}{2n_f}}, \quad (17)$$

The dimensionless bulk temperature can be defined as Eq. (18).

$$\theta_b = \frac{T_b - T_0}{T_1 - T_0} = \frac{\int_1^\lambda R U(R) \theta(R) dR}{\int_1^\lambda R U(R) dR} \quad (18)$$

Dimensionless shear stress and Nusselt number on the cylinders' wall are defined as Eqs. (19) and (20).

$$\tau|_{\text{wall}} = \frac{\mu_{nf}}{\mu_f} \frac{dU}{dR} \Big|_{\text{wall}}, \quad \begin{cases} \tau_1 = \frac{(C_1 \delta_1 + C_2 \delta_2 + 2\delta_6 + 2\delta_7) \lambda^{n_f - \delta_7 Pr S_{2f}}}{\lambda^{2n_f}} \\ \tau_2 = \frac{(C_1 \lambda^{\delta_1 - 1} \delta_1 + C_2 \lambda^{\delta_2 - 1} \delta_2 + 2\delta_6 \lambda) \lambda^{n_f - \delta_7 (Pr S_{2f} - 2n_f)} \lambda^{-\frac{Pr S_{2f} + 2n_f}{2n_f}}}{\lambda^{2n_f}} \end{cases} \quad (19)$$

Table 3 The coefficient values of CuO–water nanofluid [26]

Coefficient values	CuO–water
a_1	– 26.59331085
a_2	– 0.403818333
a_3	– 33.3516805
a_4	– 1.915825591
a_5	0.0642185846658
a_6	48.40336955
a_7	– 9.787756683
a_8	190.24561
a_9	10.92853866
a_{10}	– 0.720099837

Introducing dimensionless quantities:

$$\begin{aligned} R = \frac{r}{a}, \quad \lambda = \frac{b}{a}, \quad \theta = \frac{T - T_0}{T_1 - T_0}, \quad Z = \frac{z}{Re D_h}, \\ U = \frac{u}{u_0}, \quad P = \frac{p}{\rho_{nf} u_0^2}, \quad S = \frac{V_0 a}{v_f}, \quad Gr = \frac{g \beta_f \Delta T D_h^3}{v_f^2}, \\ Pr = \frac{v_f}{\alpha_{T,f}}, \quad Ha = BD_h \sqrt{\frac{\sigma_f}{\mu_f}}, \quad Re = \frac{u_0 D_h}{v_f}, \quad \eta = \frac{Gr}{Re}. \end{aligned} \quad (10)$$

Substituting non-dimensional parameters in Eqs. (2) and (3), the mathematical model equations and boundary conditions in dimensionless form are:

Momentum equation

$$\begin{aligned} -\frac{S}{R} \frac{d}{dR} U(R) - \frac{\mu_{nf} \rho_f}{\mu_f \rho_{nf}} \frac{1}{R} \frac{d}{dR} \left(R \frac{d}{dR} U(R) \right) \\ + \frac{1}{4(\lambda - 1)^2} \left[\frac{dP}{dZ} + \frac{Ha^2 \sigma_{nf} \rho_f}{R^2 \sigma_f \rho_{nf}} U(R) - \frac{\beta_{nf}}{\beta_f} \eta \theta(R) \right] \\ = 0 \end{aligned} \quad (11)$$

$$Nu|_{R=1} = \frac{-2(\lambda - 1) k_{eff} d\theta}{\theta|_{R=1} - \theta_b k_f dR} \Big|_{R=1} = \frac{\delta_8 \lambda^{\frac{PrS\alpha_f}{2\alpha_{nf}}}}{1 - \theta_b}, \tag{20}$$

$$Nu|_{R=\lambda} = \frac{2(\lambda - 1) k_{eff} d\theta}{\theta|_{R=\lambda} - \theta_b k_f dR} \Big|_{R=\lambda} = \frac{\delta_8}{\theta_b}$$

In which C_1 , C_2 and δ_1 – δ_8 are constant coefficients that they are defined as following:

$$C_1 = \frac{-\delta_7 \lambda^{\frac{-PrS\alpha_f + 2\alpha_{nf}}{2\alpha_{nf}}} + (-A + \delta_7 + \delta_6) \lambda^{\delta_2} - \delta_6 \lambda^2 + B}{\lambda^{\delta_1} - \lambda^{\delta_2}}$$

$$C_2 = \frac{\delta_7 \lambda^{\frac{-PrS\alpha_f + 2\alpha_{nf}}{2\alpha_{nf}}} + (A - \delta_7 - \delta_6) \lambda^{\delta_1} + \delta_6 \lambda^2 - B}{\lambda^{\delta_1} - \lambda^{\delta_2}}$$

$$\delta_1 = \frac{(1 - \lambda) S \mu_f \rho_{nf} \sigma_f + \sqrt{\mu_f (S^2 \mu_f \rho_{nf}^2 (\lambda - 1)^2 \sigma_f + Ha^2 \mu_{nf} \rho_f^2 \sigma_{nf})} \sigma_f}{2 \mu_{nf} \rho_f \sigma_f (\lambda - 1)}$$

$$\delta_2 = \frac{(1 - \lambda) S \mu_f \rho_{nf} \sigma_f - \sqrt{\mu_f (S^2 \mu_f \rho_{nf}^2 (\lambda - 1)^2 \sigma_f + Ha^2 \mu_{nf} \rho_f^2 \sigma_{nf})} \sigma_f}{2 \mu_{nf} \rho_f \sigma_f (\lambda - 1)}$$

$$\delta_3 = (\lambda - 1)^2 (\rho_f (PrS\alpha_f - 2\alpha_{nf}) \mu_{nf} - \rho_{nf} \alpha_{nf} S \mu_f) (PrS\alpha_f - 2\alpha_{nf})$$

$$\sigma_f = \frac{Ha^2 \sigma_{nf} \rho_f \mu_f \alpha_{nf}^2}{4}$$

$$\delta_4 = (\lambda - 1)^2 \left(\frac{S \mu_f \rho_{nf}}{2} + \mu_{nf} \rho_f \right) \sigma_f - \frac{Ha^2 \sigma_{nf} \rho_f \mu_f}{16}$$

$$\delta_5 = \left(-1 + \lambda^{\frac{PrS\alpha_f}{2\alpha_{nf}}} \right) \beta_f$$

$$\delta_6 = \frac{(\delta_5 \frac{dP}{dZ} + \eta \beta_{nf}) \mu_f \rho_{nf} \sigma_f}{16 \delta_4 \delta_5}$$

$$\delta_7 = \frac{-4 \eta \lambda^{\frac{PrS\alpha_f}{2\alpha_{nf}}} \alpha_{nf}^2 \beta_{nf} \mu_f \rho_{nf} \sigma_f}{16 \delta_3 \delta_5}$$

$$\delta_8 = \frac{2 k_{eff} PrS\alpha_f (\lambda - 1)}{k_f \alpha_{nf} \left(\lambda^{\frac{PrS\alpha_f}{2\alpha_{nf}}} - 1 \right)} \tag{21}$$

To demonstrate the accuracy and exactitude of the present study, the obtained exact results of this investigation for Nusselt number on inner cylinder are compared with the study of Jha et al. [27]. This comparison is carried out in the absence of a magnetic field and in the case where the Knudsen number (Kn) is zero. The mixed convection parameter (η) and Prandtl number (Pr) are considered equal to 200 and 0.7, respectively. It is also assumed that heat generation/absorption occurred in moving fluid. Figure 2 shows the results of this comparison for Nusselt number at different ratio of radii. As you can see, a very good consistency between the results is evident. In the next section, numerical results for some selected values of the parameters involved are presented.

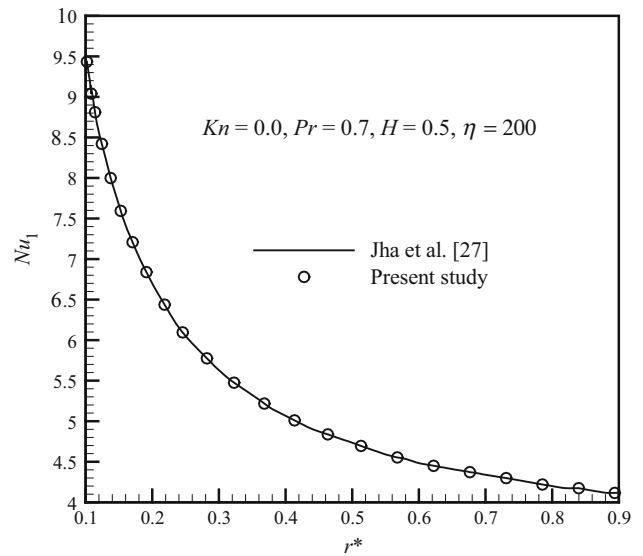


Fig. 2 Comparison of the present study’s Nusselt number on inner cylinder of annulus with Ref. [27] for $\eta = 200$, $Ha = 0$, $\eta = 200$, $H = 0.5$, $Pr = 0.7$

Results and discussion

In this study, KKL model has been used in order to estimate the nanofluid properties by considering Brownian motion. Thus, such active parameters as Hartman number (Ha), shape factor (n), volume fraction of nanoparticles (ϕ), Nusselt number (Nu), radial ratio (λ), mixed convection parameter (η) and suction/injection parameter (S) have been investigated through the exact solution of the governing equations.

In Table 4, different values of the Nusselt number for different shapes of nanoparticles are presented. As you can see, on both internal and external cylinders the platelet and spherical have the highest and lowest Nusselt numbers, respectively. As a result, CuO nanoparticles with a platelet shape have been used to achieve an optimal heat transfer.

Table 5 shows the impact of increase in the volume fraction on the Nusselt number of the internal and external cylinders’ walls in two cases: with and without taking the

Table 4 Effect of shape of nanoparticles on Nusselt number when $\eta = 5$, $\lambda = 2$, $S = 1$, $A = 1$, $B = 0$ and $\phi = 0.04$

	Nu_1		Nu_λ	
	$Ha = 0$	$Ha = 20$	$Ha = 0$	$Ha = 20$
Spherical	16.7416	15.6222	1.5913	2.0013
Brick	16.8538	15.7156	1.6466	2.0696
Cylinder	17.0213	15.8549	1.7299	2.1717
Platelet	17.1502	15.9626	1.7944	2.1717

Table 5 Comparison of Nusselt number enhancement on the walls of internal and external cylinders for different volume fractions in two cases: with and without taking the effect of Brownian motion into consideration in $Ha = 2, \lambda = 2, S = 0, A = 1, B = 0$ and $\eta = 5$

ϕ	With Brownian motion		Without Brownian motion	
	Nu_1	Nu_λ	Nu_1	Nu_λ
0.00	5.5198	3.0228	5.5198	3.0228
0.01	5.8643	3.2105	5.7848	3.1670
0.02	6.6413	3.6349	6.0544	3.3136
0.03	7.5846	4.1501	6.3285	3.4627
0.04	8.6375	4.7252	6.6074	3.6144
0.05	9.7732	5.3455	6.8911	3.7687

effect of Brownian motion into consideration. The volume fraction of nanoparticles has changed in the range of 0.01–0.05, and the situation in which the pure water is used ($\phi = 0$) has also been investigated. As it can be observed, with the increase in the volume fraction of nanoparticles in the base fluid, the heat advection of the hot wall also increases due to a rise in the nanofluid’s thermal conductivity and better heat diffusion. As a result, the Nusselt number increases on both walls. Furthermore, the obtained values for the Nusselt number are clearly more than the model of constant properties when the effects of Brownian motion are taken into account. For example, with and without taking the effect of Brownian motion into consideration, the percentage of Nusselt number enhancement on internal cylinder’s wall, for nanofluid with volume fraction of $\phi = 0.04$ in comparison with the situation in which the pure water is employed, is equal to 56.49 and 19.70%, respectively. It is worth mentioning here that the results correspond with what Pak and Cho [28], Xuan and Li [29] and He et al. [30] have achieved.

It should be noted that the results obtained in the paper will be presented hereafter for the nanofluid with volume fraction of $\phi = 0.04$.

As mentioned, the surface of the internal and external cylinders is perforated, and according to Fig. 1, $S > 0$ represents the state that injection occurs in the cylinder wall toward the annulus axis. $S < 0$ also shows the opposite of the above-mentioned state. Figure 3 shows the changes in the dimensionless temperature of the nanofluid inside the annulus for different values of the suction/injection parameter. Since the temperatures of internal cylinder are higher than the temperature of nanofluid, heat transfer takes place between the cylinder’s wall and the nanofluid and as a result the nanofluid temperature heightens. If $S > 0$, the temperature of the nanofluid near the hot wall (internal cylinder) decreases. The temperature

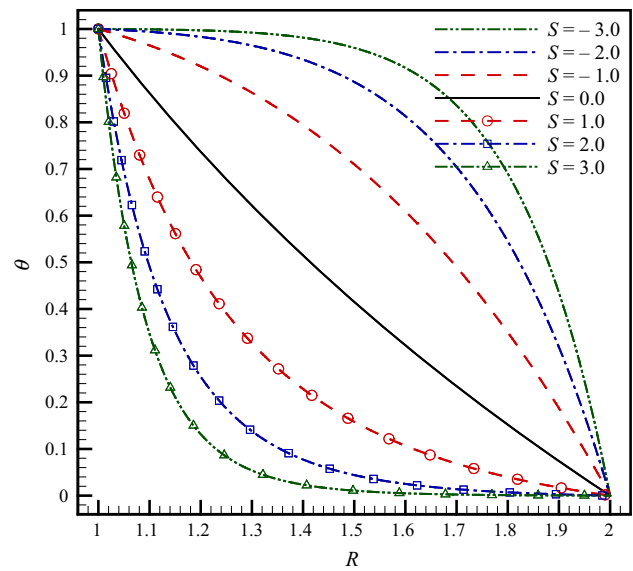


Fig. 3 Dimensionless temperature profile inside the annulus in different values of the suction/injection parameter for $\lambda = 2$

decreases with the increase in S . But, if $S < 0$, then these results will be just opposite.

Figure 4 illustrates the changes of fully developed dimensionless velocity in diverse situations at which each of the internal and external cylinders moves either in the same or contrary direction of z axis. As it can be perceived in Fig. 4a, b, of two walls, one of them is stationary and the other wall moves at a constant velocity. In Fig. 4c, it is apparent that both cylinders move at a uniform velocity. As previously noted, the volumetric flow rate of nanofluid is assumed to be constant at any cross section of annulus. Accordingly, owing to the movement of cylinder’s wall in the contrary direction of z axis, the volumetric flow rate of nanofluid diminishes. In this respect, the recompense of its values is fulfilled by increasing the nanofluid velocity and pressure difference. But then, augmenting the values of wall velocity in the direction of z axis leads the maximum velocity to decline and makes the velocity profile get close to the moving wall. However, the situation in which the wall of cylinder moves in the contrary direction of z axis reveals the reverse results. It is noteworthy that Fig. 4d also depicts the different wall motion states and its effect on the dimensionless velocity profile. As it can be seen, due to the application of magnetic field, a turning point is created in the graph of fully developed dimensionless velocity profile when the external cylinder is stationary and the wall of internal cylinder moves in the positive direction of z axis. The aforesaid magnetic force causes Lorentz force to overcome the Buoyancy force and reduce the velocity near the internal cylinder.

Figure 5 shows the variation of the fully developed dimensionless velocity, with diverse Hartman numbers for

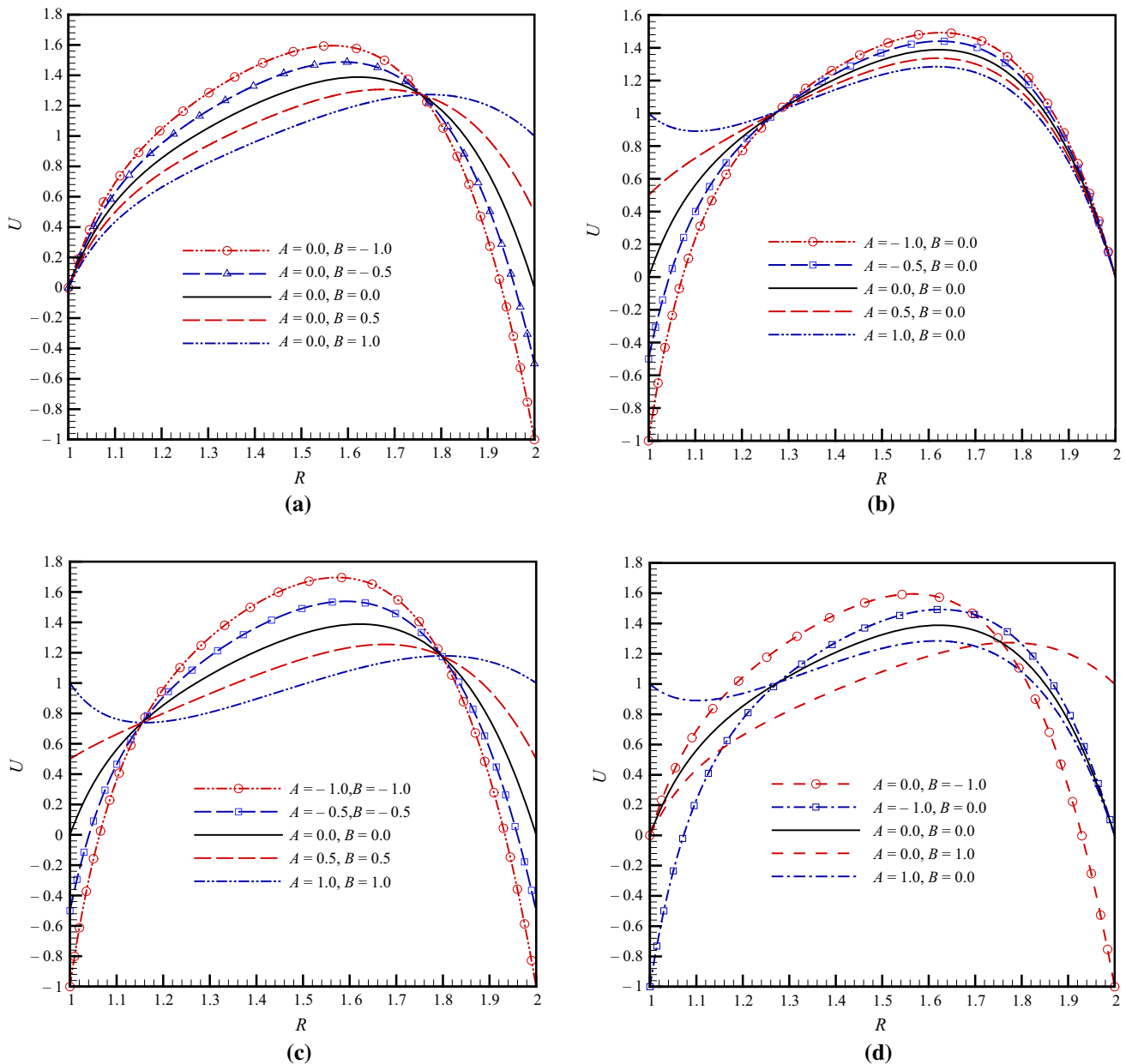


Fig. 4 Effect of the velocity variations of annulus's internal and external cylinders on the nanofluid dimensionless fully developed velocity profile in $\eta = 5$, $S = 1$, $Ha = 20$ and $\lambda = 2$

various modes of movement of external and internal cylinders.

In Fig. 5a–c when there is no magnetic field, the fully developed velocity profile has parabolic form and the maximum velocity occurs in the left side of gap between cylinders of annulus owing to the domination of Buoyancy force. But with the application of a radial magnetic field, Lorentz force is applied axially to the nanofluid flow; as a result, the velocity gradient increases near the walls, and the velocity profile takes a flattened form. Since the radial magnetic field that is applied to the nanofluid flow has an

opposite relationship with radius ($B_0 a/r$), a higher Lorentz force is on the nanofluid near the internal cylinder and its effect will be reduced by approaching the external cylinder. According to Fig. 5c, as the internal cylinder is moving in the absence of a magnetic field, the point at which the maximum velocity occurs will be adjacent to the hot wall. But when the magnetic field strength increases and the Lorentz force overcomes the buoyancy force and the momentum, the profile of the velocity is flattened. In Fig. 5d, two extremum points are created due to the movement of both walls.

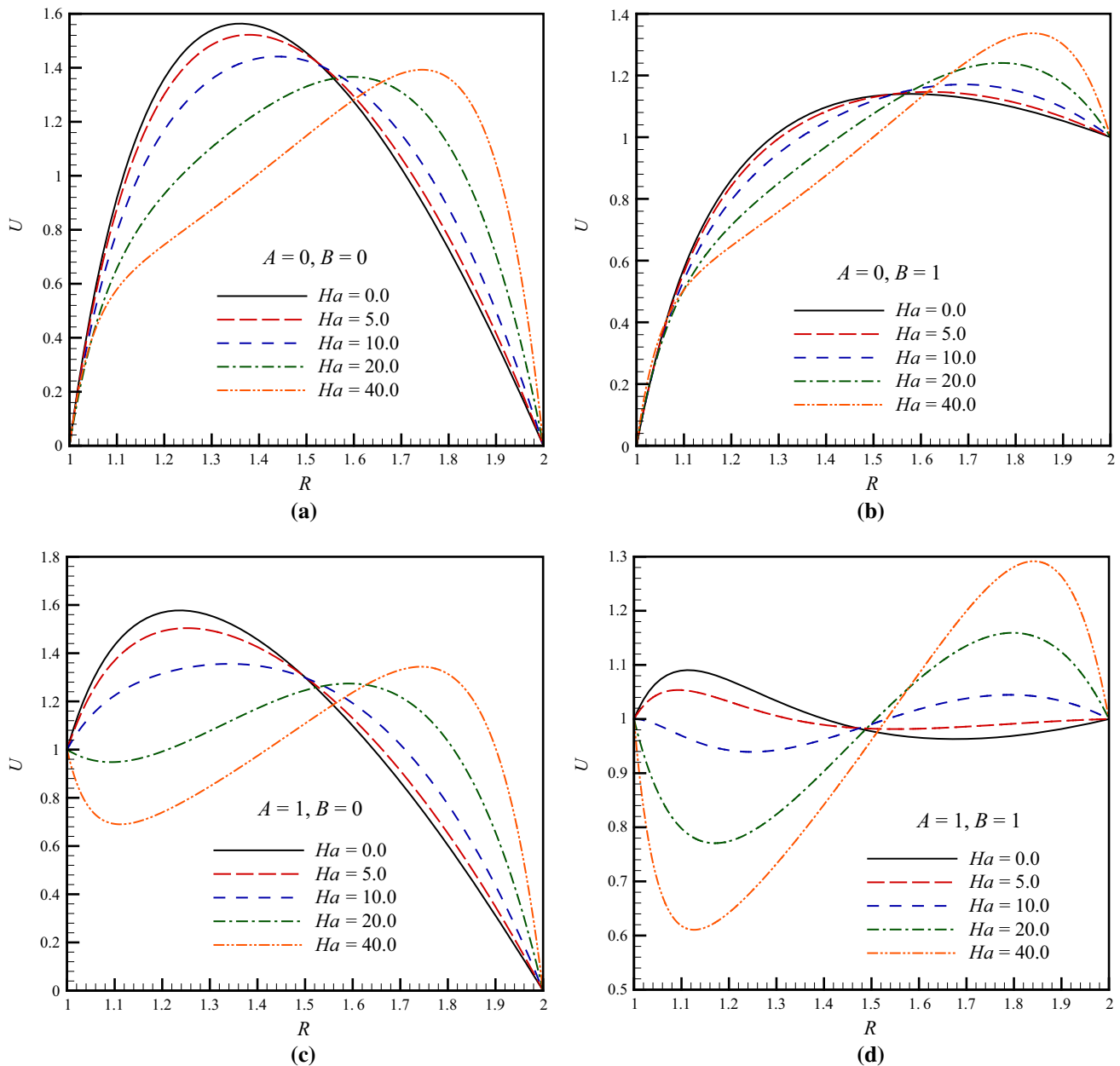


Fig. 5 Variations of nanofluid’s fully developed dimensionless velocity for different Hartman numbers and various states of the cylinders’ motion in $\eta = 100, S = 3$ and $\lambda = 2$

In Fig. 6a–d, the effect of S parameter’s variations on the dimensionless velocity of nanofluid has been presented for different modes of movement of external and internal cylinders. As you can see, the presence of suction/injection on the wall of internal and external cylinders will cause some changes in velocity profile. According to Fig. 6a–c in case of $S > 0$ in comparison with the time when suction/injection is not present, the maximum points in the velocity profile will move toward the internal wall. In other words, nanofluid injections increase the velocity in the vicinity of the internal cylinder. The opposite of this situation will

happen in case of $S < 0$. In Fig. 6d, in the case of both cylinders moving together, the velocity profile will have two extremum points, unlike other modes. These two points are due to the uniform movement of both cylinders.

The minimum velocity point is created near the hot wall of internal cylinder due to the domination of Lorentz force over buoyancy force.

Since the intensity of magnetic field has an opposite relationship with the radial distance, the maximum velocity will occur in the vicinity of the external cylinders’ wall; therefore, the graph has a turning point.

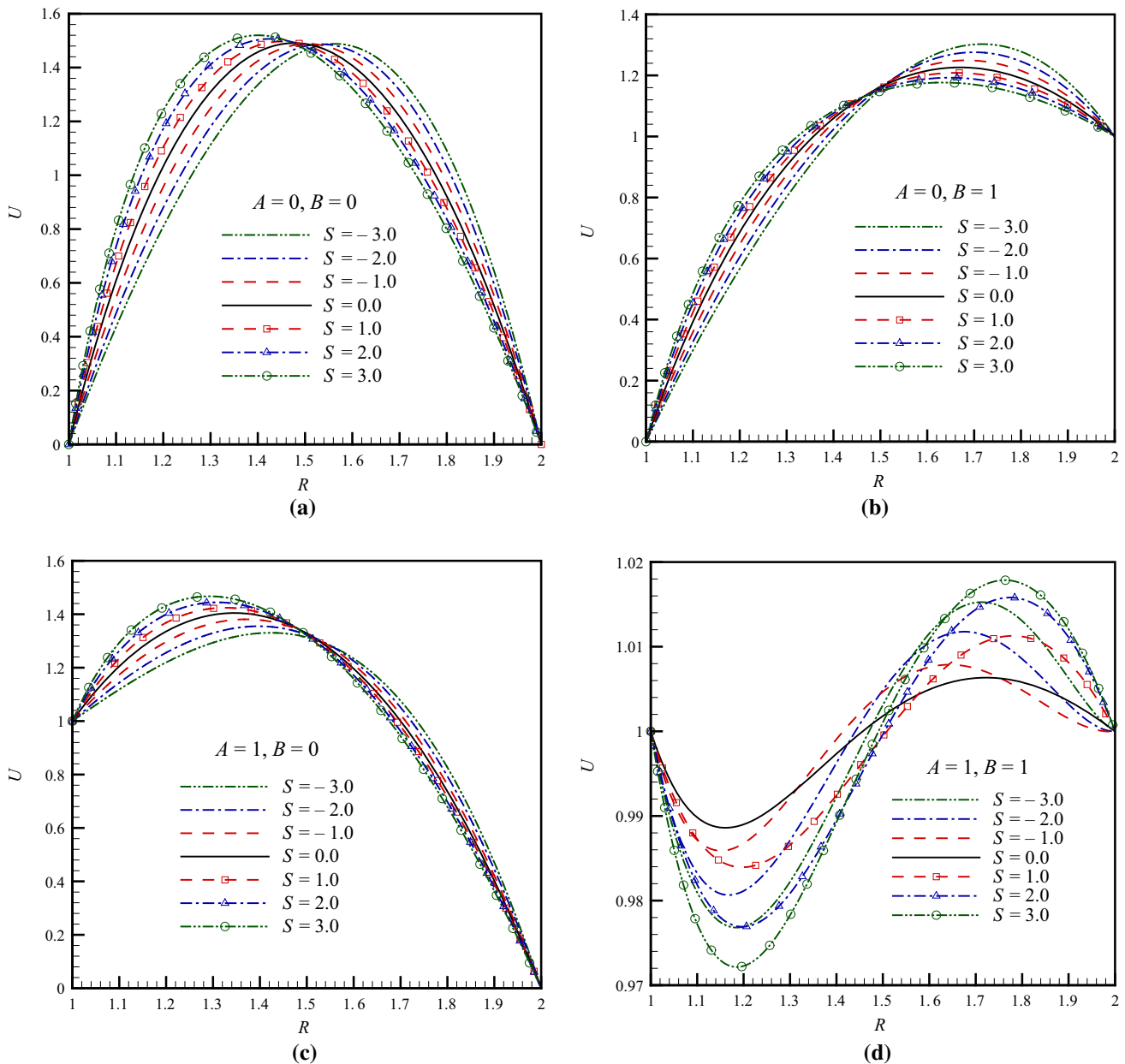


Fig. 6 Effects of suction/injection variation on dimensionless velocity in different modes of internal and external cylinders' movements for $\eta = 5$, $Ha = 10$ and $\lambda = 2$

Figure 7 illustrates the effects of mixed convection parameter's variation on the fully developed dimensionless velocity for different modes of internal and external cylinders' movements. As it is noticed, with the increase in the mixed convection parameter, the buoyancy force reinforced and the nanofluid velocity will increase significantly in the adjacent hot wall. In the case when both walls move together, the nanofluid in the hot wall initially has a minimum velocity, which is due to the application of radial magnetic field and Lorentz force's power over the Buoyancy force. But as the mixed convection parameter

increases, the Buoyancy force will be more than Lorentz force and the velocity of the nanofluid near the hot wall increases.

The effect of variations of mixed convection parameter on the Nusselt number in various situations when both cylinders have different moving states is shown in Fig. 8. These movements could be in the same direction or in the opposite direction of z axis. As of Eq. (20), the ratio of convection heat transfer to the conductive heat transfer which can be calculated on the walls of both cylinders defines the Nusselt number. As it can be noted, by

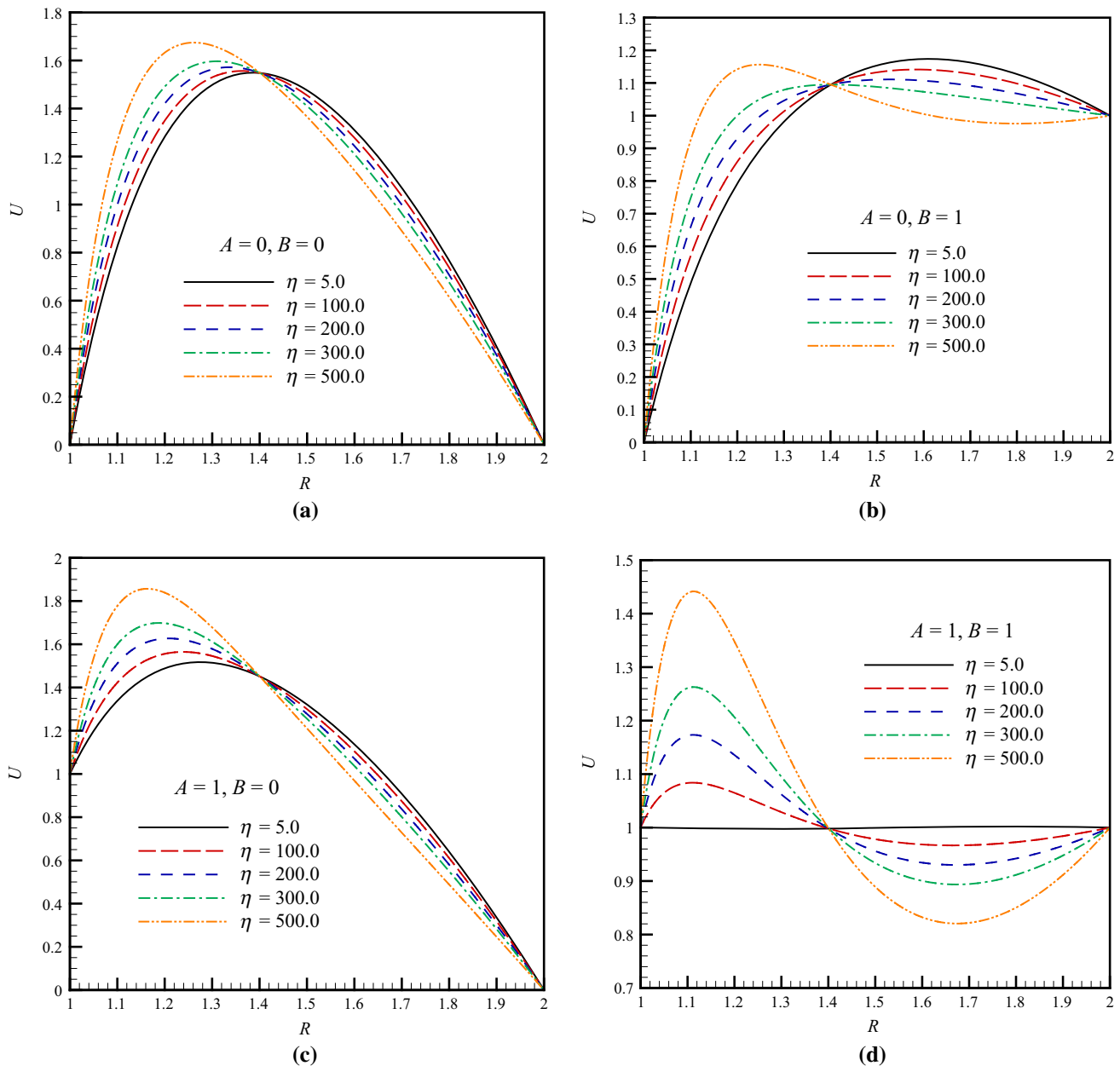
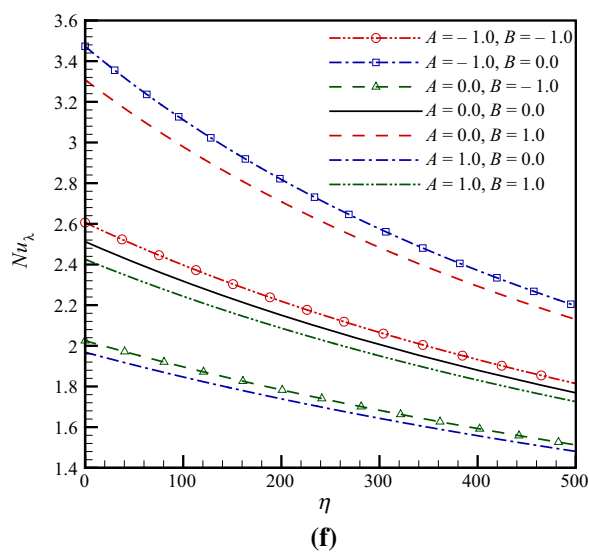
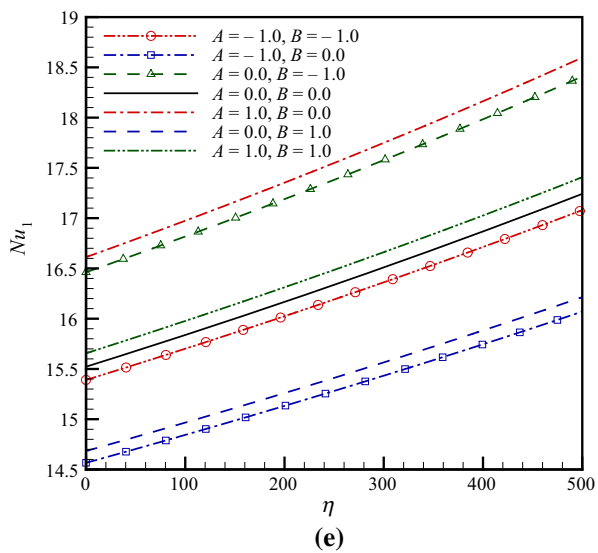
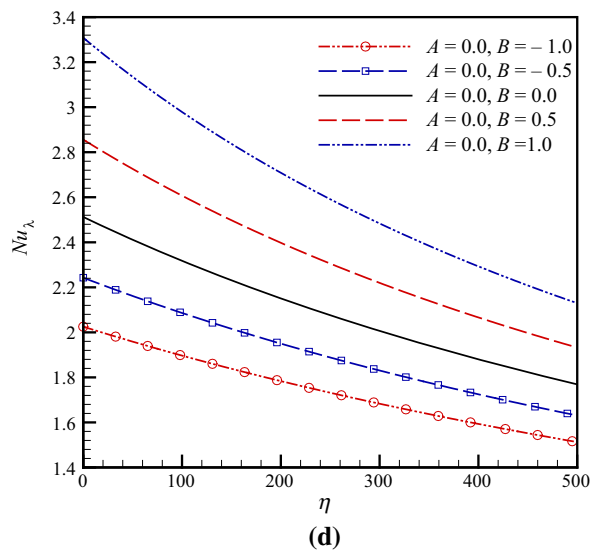
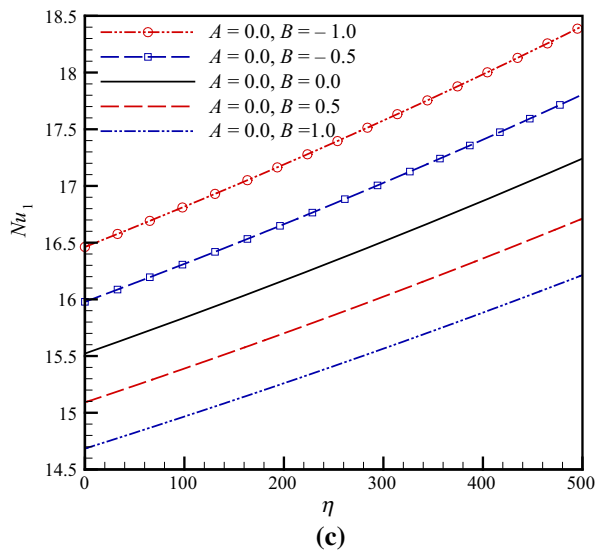
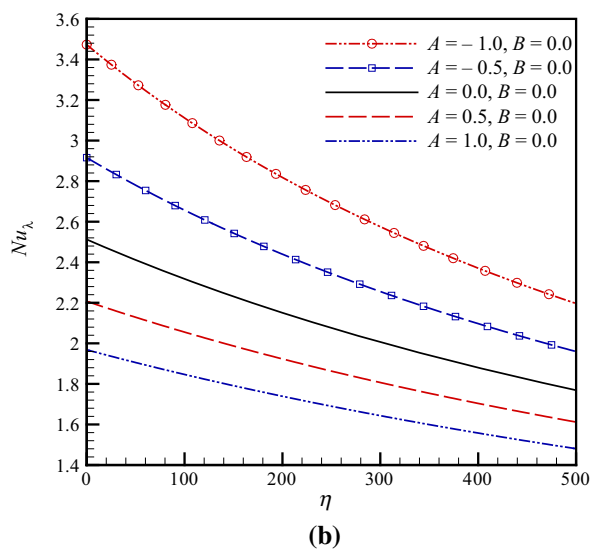
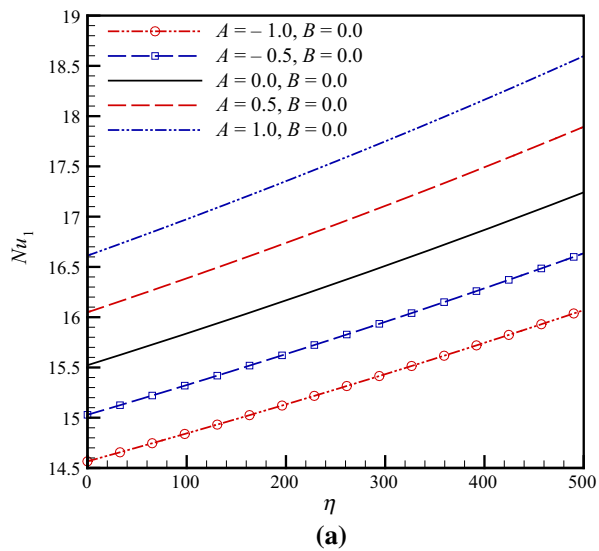


Fig. 7 Effects of mixed convection parameter’s variation on dimensionless velocity in different modes of internal and external cylinders’ movements for $Ha = 2, S = 3$ and $\lambda = 2$

enhancing η near the wall of internal cylinder the buoyancy force is reinforced and it causes increase and decrease in Nusselt number on the walls of internal and external cylinders, respectively, for different states of cylinder’s walls movements. One wall is stationary, and the other one moves at a constant velocity in results presented in Fig. 8a–d. The Nusselt number increases and decreases, respectively, on the walls of internal and external cylinders when the velocity of internal wall goes from negative to positive values. Variations of the speed of the external wall develop the inverse of the above outputs. Different modes of

cylinders’ walls and its effects on the Nusselt number are depicted in Fig. 8e, f. It is worth mentioning that for stationary external cylinder and moving internal cylinder in the direction of z axis, the maximum and minimum heat transfer take place on the internal and external walls, respectively.

Figure 9 depicts the graph of Nusselt number variations on the walls of internal and external cylinders in various radial ratios and different suction/injection parameters. According to Fig. 9, the enhancement of S parameter in internal cylinder causes to increase Nusselt number.



◀ **Fig. 8** Effect of the variations of mixed convection parameter on the Nusselt number for different states of internal and external cylinders' movements for $Ha = 10$, $S = 1$ and $\lambda = 2$

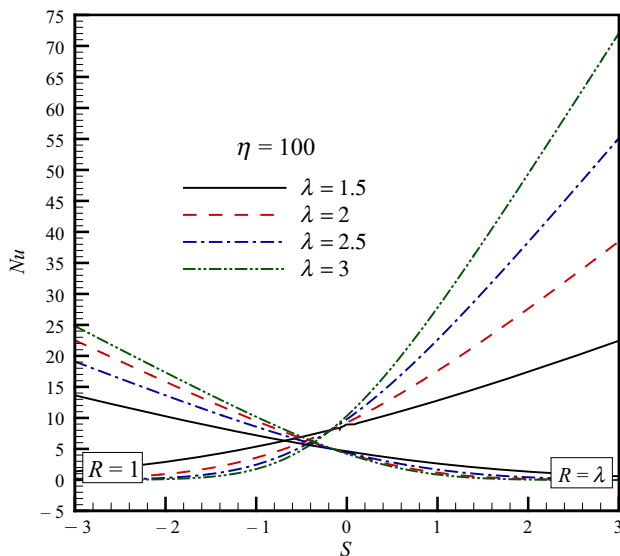


Fig. 9 Investigation of Nusselt number in different radial ratios and various suction/injection parameter, for $A = 1$, $B = 0$, $\eta = 100$ and $Ha = 2$

Moreover, as it can be seen, for internal cylinder the Nusselt number decreases by enhancing λ in negative S parameter, and it increases by augmenting λ in positive S parameter. It should be mentioned here that the achieved results show the reverse consequences regarding the external wall.

It is shown in Fig. 10 how shear stress is affected by variation of mixed convection parameter, while cylinders walls are moving in different situations. Shear stress being directly related to the velocity gradient, then mixed convection parameter's enhancement reinforces the buoyancy force and the velocity gradient near the hot wall (internal cylinder). Therefore, the shear stress gets larger depending on different modes of internal and external cylinders' movement. It is not too far reaching to expect that the highest value of the shear stress happens when the cylinders move in the opposite direction of z axis and it is the lowest when both the cylinders move at a constant velocity and in the same direction of z axis. It can easily be concluded that the reverse of these issues takes place for the shear stress on the external cylinder.

Figure 11 shows the effects of radial ratio changes between two cylinders (λ), Hartmann number (Ha) and suction/injection parameter on the shear stress of nanofluid on the internal cylinder's wall.

It is evident that in the absence of a magnetic field, along with the increase in S parameter, the shear stress

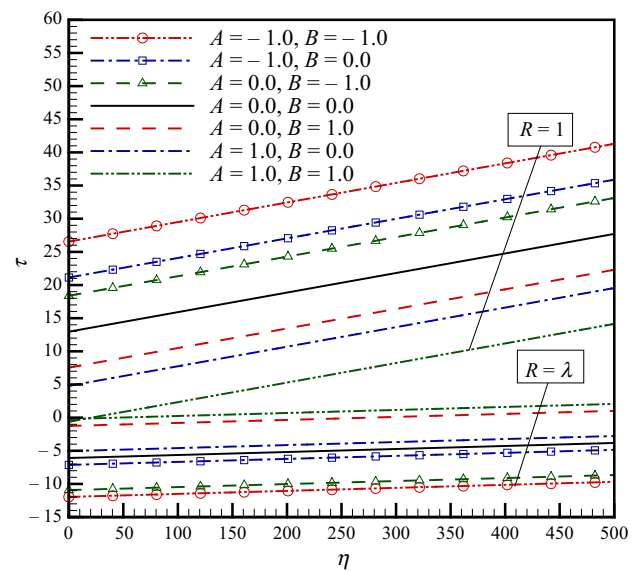


Fig. 10 Effects of changing mixed convection parameter on shear stress in different states of internal and external cylinders' movement for $S = 3$, $Ha = 5$ and $\lambda = 2$

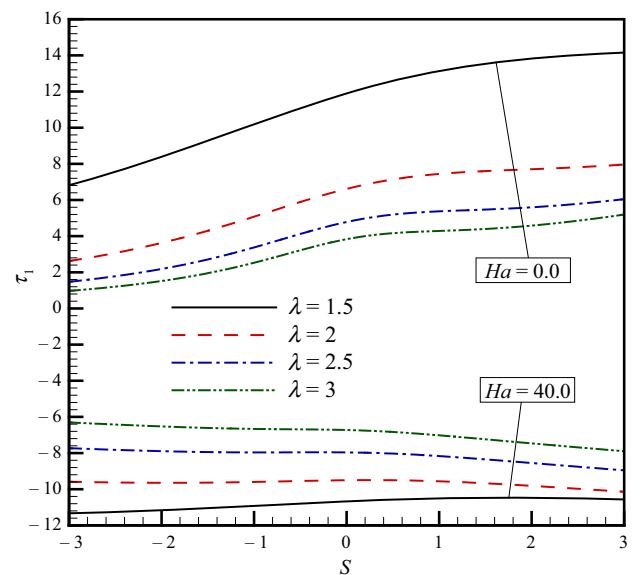


Fig. 11 Effects of radial ratio variations between two cylinder (λ) and S parameter on shear stress in different intensities of magnetic field for $R = 1$, $A = 1$, $B = 0$ and $\eta = 100$

increases on the wall of cylinders. As it can be observed, the slope of surface tensions' variation for negative S is more than positive ones. However, the presence of radial magnetic field makes Lorentz force control the flow, and as the S parameter increases, shear stress decreases. In addition, as it is perceived, the application of the magnetic field results in a negative velocity gradient and shear stress. According to Fig. 11, with the increase in λ , the velocity

gradient decreases in the vicinity of the internal cylinder wall and decreases the shear stress.

Conclusions

This paper has presented the exact solution of CuO–water nanofluid's MHD mixed convective flow in a vertical cylindrical annulus with moving walls, for the first time, which is in the vicinity of the radial magnetic field. Considering the Brownian motion and the shaped factor effect, this paper has provided its readers with such graphs as Nusselt numbers, shear stress, temperature and velocity in different values of radial ratio, volume fraction, suction/injection parameter, mixed convection parameter and Hartmann number for diverse modes of cylinders' movement. The results showed that increasing the nanoparticles volume fraction resulted in a high rate of heat transfer, and the nanoparticles in the shape of platelet have the highest rate. The results shed light on the fact that injection ($S > 0$) heightens the velocity of fluid in the adjacency of internal cylinder's wall. In this regard, the Nusselt number also increases on the wall of internal cylinder with the enhancement of S parameter. Besides, the growth of mixed convection parameter (η) reinforces the buoyancy force and increases the fluid velocity in the vicinity of internal cylinder's wall. In this way, the shear stress and the Nusselt number increase on the wall of internal cylinder in various situations of cylinders' movements. The results indicated that if the internal cylinder is stationary and the external cylinder moves in the opposite direction of z axis, the maximum and minimum heat transfer happen on the walls of internal and external cylinders, respectively. In addition, the results will be reversed for the Nusselt number if the external cylinder is stationary and the internal cylinder moves in the direction of z axis at a uniform velocity. The results showed that by exerting radial magnetic field, the Lorentz force is applied to the nanofluid flow axially and it makes the velocity profile take a flat shape. On the one hand, in the absence of magnetic field for the internal cylinder's wall, the shear stress is increased with the augmentation of S parameter, and on the other hand, the shear stress diminishes in the presence of magnetic field. The results also revealed that the growth of λ lessens the shear stress and augments the Nusselt number on the wall of internal and external cylinders. As a result, using the methods presented in this paper, the flow and heat transfer rate of the nanofluid in the vertical cylindrical annulus can be controlled.

Acknowledgement Hereby, the financial support of Ferdowsi University of Mashhad under contract No. 2/46663 is acknowledged during accomplishment of this research.

References

1. Singh S, Jha B, Singh A. Natural convection in vertical concentric annuli under a radial magnetic field *Natürliche Konvektion in vertikalen, konzentrischen Ringspalten unter Einwirkung eines radialen Magnetfeldes*. *Heat Mass Transf.* 1997;32(5):399–401.
2. Avcı M, Aydın O. Mixed convection in a vertical microannulus between two concentric microtubes. *J Heat Transf.* 2009;131(1): 014502.
3. Rahimi AB, Abedini A. Numerical study of three-dimensional mixed convection in an eccentric annulus. *J Thermophys Heat Transf.* 2013;27(4):719–32.
4. Jha BK, Aina B, Muhammad S. Combined effects of suction/injection and wall surface curvature on natural convection flow in a vertical micro-porous annulus. *Thermophys Aeromech.* 2015; 22(2):217–28.
5. Shakiba A, Rahimi AB. Mixed convective flow of electrically conducting fluid in a vertical cylindrical annulus with moving walls adjacent to a radial magnetic field along with transpiration. *J Fluids Eng.* 2019;141:081111.
6. Saidur R, Leong K, Mohammad H. A review on applications and challenges of nanofluids. *Renew Sustain Energy Rev.* 2011;15(3): 1646–68.
7. Bianco V, Vafai K, Manca O, Nardini S. Heat transfer enhancement with nanofluids. Boca Raton: CRC Press; 2015.
8. Shakiba A, Vahedi K. Numerical analysis of magnetic field effects on hydro-thermal behavior of a magnetic nanofluid in a double pipe heat exchanger. *J Magn Magn Mater.* 2016;402:131–42.
9. Jha BK, Aina B, Ajiya A. Role of suction/injection on MHD natural convection flow in a vertical microchannel. *Int J Energy Technol.* 2015;7(2):30–9.
10. Freidoonimehr N, Rahimi AB. Exact-solution of entropy generation for MHD nanofluid flow induced by a stretching/shrinking sheet with transpiration: dual solution. *Adv Powder Technol.* 2017;28(2):671–85.
11. Mozayeni H, Rahimi AB. Unsteady mixed convection with heating effects in a horizontal annulus with constant rotating outer cylinder and constant magnetic field. In: 13th Annual and 2nd international fluid dynamics conference; 2010.
12. Mozayeni H, Rahimi A. Mixed convection in cylindrical annulus with rotating outer cylinder and constant magnetic field with an effect in the radial direction. *Sci Iran.* 2012;19(1):91–105.
13. Mahian O, et al. Recent advances in modeling and simulation of nanofluid flows—part I: fundamentals and theory. *Phys Rep.* 2018. <https://doi.org/10.1016/j.physrep.2018.11.004>.
14. Mahian O, et al. Recent advances in modeling and simulation of nanofluid flows—part II: applications. *Phys Rep.* 2018. <https://doi.org/10.1016/j.physrep.2018.11.003>.
15. Malvandi A, Ganji DJP. Mixed convection of alumina–water nanofluid inside a concentric annulus considering nanoparticle migration. *Particuology.* 2016;24:113–22.
16. Dogonchi AS, Ganji DD. Thermal radiation effect on the nanofluid buoyancy flow and heat transfer over a stretching sheet considering Brownian motion. *J Mol Liq.* 2016;223:521–7.
17. Chon CH, Kihm KD, Lee SP, Choi SU. Empirical correlation finding the role of temperature and particle size for nanofluid (Al_2O_3) thermal conductivity enhancement. *Appl Phys Lett.* 2005;87(15):153107.
18. Khanafer K, Vafai K. A critical synthesis of thermophysical characteristics of nanofluids. *Int J Heat Mass Transf.* 2011;54(19): 4410–28.
19. Koo J, Kleinstreuer C. A new thermal conductivity model for nanofluids. *J Nanopart Res.* 2004;6(6):577–88.
20. Xuan Y, Li Q, Hu W. Aggregation structure and thermal conductivity of nanofluids. *AIChE J.* 2003;49(4):1038–43.

21. Koo J, Kleinstreuer C. Viscous dissipation effects in microtubes and microchannels. *Int J Heat Mass Transf.* 2004;47(14–16): 3159–69.
22. Koo J, Kleinstreuer C. Laminar nanofluid flow in microheat-sinks. *Int J Heat Mass Transf.* 2005;48(13):2652–61.
23. Li J. Computational analysis of nanofluid flow in microchannels with applications to micro-heat sinks and bio-MEMS, PhD thesis, North Carolina State. <http://www.lib.ncsu.edu/resolver/1840.16/4749>.
24. Selimefendigil F, Öztop HF. Analysis of MHD mixed convection in a flexible walled and nanofluids filled lid-driven cavity with volumetric heat generation. *Int J Mech Sci.* 2016;118:113–24.
25. Selimefendigil F, Öztop HF. Magnetic field effects on the forced convection of CuO–water nanofluid flow in a channel with circular cylinders and thermal predictions using ANFIS. *Int J Mech Sci.* 2018;146:9–24.
26. Li J, Kleinstreuer C. Thermal performance of nanofluid flow in microchannels. *Int J Heat Fluid Flow.* 2008;29(4):1221–32.
27. Jha BK, Oni MO, Aina B. Steady fully developed mixed convection flow in a vertical micro-concentric-annulus with heat generating/absorbing fluid: an exact solution. *Ain Shams Eng J.* 2016. <https://doi.org/10.1016/j.asej.2016.08.005>.
28. Pak BC, Cho YI. Hydrodynamic and heat transfer study of dispersed fluids with submicron metallic oxide particles. *Exp Heat Transf Int J.* 1998;11(2):151–70.
29. Xuan Y, Li Q. Investigation on convective heat transfer and flow features of nanofluids. *J Heat Transf.* 2003;125(1):151–5.
30. He Y, Jin Y, Chen H, Ding Y, Cang D, Lu H. Heat transfer and flow behaviour of aqueous suspensions of TiO₂ nanoparticles (nanofluids) flowing upward through a vertical pipe. *Int J Heat Mass Transf.* 2007;50(11):2272–81.

Publisher's Note Springer Nature remains neutral with regard to jurisdictional claims in published maps and institutional affiliations.